Electronic Supplementary Material (ESI) for Chemical Communications
This journal is © The Royal Society of Chemistry 2013

**Electronic Supplemental Information**

# Sequential Binding of Large Molecules on Hairy MOFs

Gonghua Wang,[a] Zhanping Xu, [a] Ziguang Chen, [a] Wei Niu, [b] You Zhou,[c] Jiantao Guo, [b] Li Tan*[a]

[a] *Department of Mechanical and Materials Engineering, University of Nebraska, Lincoln, Nebraska 68588, United States Tel: 014024724018; E-mail: ltan4@unl.edu*
[b] *Department of Chemistry, University of Nebraska, Lincoln, Nebraska 68588, United States*
[c] *Center for Biotechnology, University of Nebraska, Lincoln, Nebraska 68588, United States*

## 1. Materials

In our experiments, Cu(FMA)(4,4'-Bpe)$_{0.5}$·0.5$H_2O$ (Cu-MOFs) were used, where FMA is fumarate ion ($C_4H_2O_4^{2-}$) and 4,4'-Bpe is 4,4'-vinylenedipyridine ($C_{12}H_{10}N_2$). Cu-MOFs were synthesized after an established "shake-and-bake" method.[S1] Briefly, a mixed solution of $Cu(NO_3)_2$·2.5$H_2O$ (0.0663 g, 0.285 mmol), $H_2$FMA (0.0331 g, 0.285 mmol), and 4, 4'-Bpe (0.0260 g, 0.143 mmol) in $H_2O$ (25 mL) in a 30 mL glass vial was heated in a convection oven (DKN400, Yamato Scientific America, Inc.) at 100 °C for 24 h. The greenish Cu-MOF crystals (~ 40% yield) were obtained after a copious filtration, hot water rinsing, and air drying. Cu-MOF-1 was obtained by soaking Cu-MOF in an aqueous NaCl solution (57 mM) and the following filtration, repeated rinsing and air drying. $CuCl_2$·(4,4'-Bpe) was synthesized as an effort towards identifying hairy MOFs. Anhydrous $CuCl_2$ (0.148 g, 1.10 mmol) and 4, 4'-Bpe (0.100 g, 0.55 mmol) was mixed, added with 30 ml of deionized water, the mixture was heated in a convection oven at 100 °C for 24 h. The $CuCl_2$·(4,4'-Bpe) complex powders were obtained after filtration, rinsing and drying. CuFMA was synthesized according to an established method.[S2] In a typical synthesis, $CuCO_3$·$Cu(OH)_2$ (0.0144 g, 0.0651 mmol) and $H_2$FMA (0.0758 g, 0.653 mmol) was added to 10 ml of deionized water, heated in a convection oven at 100 °C for 24 h. Light blue CuFMA powders were collected after filtration, rinsing and drying process.

Protein adhesion tests were performed using GFPs ($GFP_{uv}$ with excitation wavelength of 395 nm and emission wavelength of 510 nm) and RFPs (m-cherry with excitation wavelength of 587 nm and emission wavelength of 610 nm). Both proteins, stored in potassium phosphate buffer (50 mM, pH 7.4), were expressed with a hexahistidine tag, which can enhance their binding with metal sites. The interaction between GFPs and the copper compounds were probed by soaking the Cu compounds (Cu-MOF, Cu-MOF-1, $CuCl_2$·(4,4'-Bpe) and CuFMA) in an aqueous solution of GFPs (~3.0 μg/mL) for 1 week at 4 °C, followed by examination using confocal fluorescence microscope. The controlled salt etching process was revealed by alternate RFPs and GFPs staining. The CuMOF crystals were first etched with NaCl solution (57 mM) for 1 day, after removing the solution, the solid was soaked in RFP solution for 1 week, followed by a second NaCl etching, washing and soaking in GFPs solution. Dulbecco's Modified Eagle Medium (DMEM) with added fetal bovine serum (FBS) was prepared according to manufacture's instruction (Life Technologies, Carlsbad, CA).

## 2. Characterizations

X-ray diffractometry (XRD, Bruker AXS D8 Discover with GADDS) was conducted to examine the crystal structures of Cu-MOF, Cu-MOF-1, $CuCl_2$·(4,4'-Bpe) and CuFMA samples. The weighted average wavelength of the CuKα x-ray source was 1.5417 Å. Atomic force microscopy (AFM, Dimension 3100 SPM system) was performed to reveal the surface morphology of the Cu-MOFs, crushed Cu-MOFs and its morphological developments in salt solutions with various concentrations. Before AFM imaging, the Cu-MOF crystals were soaked in the salt solutions for 10 minutes before washing and drying. The Scanning Probe Image Processor software (SPIP, Image Metrology, Denmark) was used to analyze the surface roughness and depth profiles. Optical images of the Cu-MOF were taken with an optical microscope (Meiji ML8000) equipped with a digital camara (Moticam 2000). The GFPs-containing samples were examined with a 60× (PlanApo/1.45) oil lens and imaged with an Olympus FV500-IX81 confocal laser scanning microscope system using the 488 nm excitation laser line (Olympus America Inc., Center Valley, PA). For the samples with both GFPs and RFPs, images were collected using the sequential mode using 488 nm/543 nm

excitations and 520 nm/595 nm emissions, respectively. Elemental analysis of $CuCl_2$·(4,4'-Bpe) was performed in Atlantic Microlab, Inc. (Norcross, GA). Gas sorption isotherms of H-MOFs were collected using the surface area analyzer ASAP-2020 (Micromeritics, Norcross, GA). $N_2$ sorption isotherms were measured at 77 K with liquid nitrogen; $CO_2$ sorption isotherms were measured at 195 K with an acetone/dry ice slush. Before sorption measurements, the sample was vacuumed at 150 °C for 6 hours.

**3. Crystal structure of Cu-MOFs**

The Cu-MOFs are assembled in an interpenetrating pseudo-cubic crystal structure, with the (200) layers composed of pure Cu-O bonds, and pillar-like 4,4'-Bpe units between the (200) layers[1] (Table S1, Fig. S1). Since the binding energy of Cu-N bond (90 kJ/mole) is much lower than that of Cu-O bond (186 kJ/mole), the (200) planes have a smaller inter-plane strength. Essentially, the inter-planar pillar linkers are weaker than the in-plane carboxylate moieties, therefore when mechanically crushed, the fragile Cu-N bonds that connect the (200) planes are easier to break, likely leaving dangling 4,4'-Bpe and coordinatively unsaturated Cu atoms (Fig. 1).

**Table S1.** Major planes in Cu-MOFs and their anisotropy in composition and strength.

| Experimental XRD (2θ) Position | Simulated XRD (2θ) Position | Crystal Plane | Area ($A^2$) | No. of Inter-layer Bonds (Cu-O, Cu-N) | Interlayer Strength ($kJ/N_A \cdot A^2$) | In-plane Strength ($kJ/N_A \cdot A^2$) |
|---|---|---|---|---|---|---|
| 11.175° | 11.174° | (2 0 0) | 146.18 | (0, 2) | 1.23 | 18.28 |
| 12.687° | 12.672° | (1 1 1) | 167.28 | (4, 2) | 5.07 | 7.99 |
| 13.610° | 13.601° | (0 0 2) | 160.15 | (8, 0) | 8.34 | 2.25 |
| 16.011° | 16.011° | (0 2 0) | 214.53 | (8, 0) | 6.23 | 1.68 |
| 21.066° | 21.066° | (0 2 2) | 277.44 | (4, 0) | 2.41 | 6.11 |

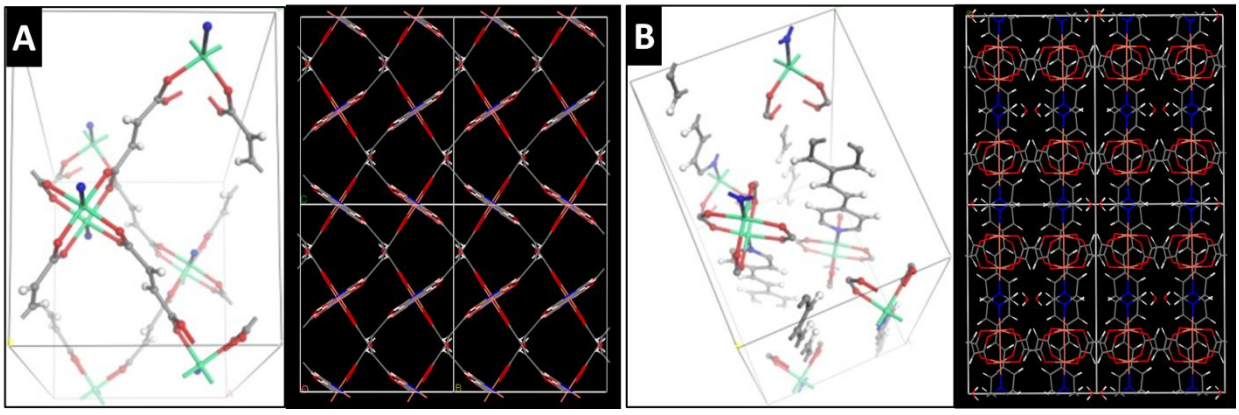


**Figure S1.** Anisotropic structure of Cu-MOFs. (A) Selected view of the (200)s in a box, with its plane view on the right. Each knots (red cross) is composed of 2 copper atoms (in green) that are coordinated with 8 oxygen atoms (in red) from the acid (in gray) to form a continuous network; and (B) simplified (002)s in a box, with its plane view on the right. Each pillar in the box is composed of nitrogen atoms (in blue) that are coordinated with copper from the top or bottom.

This journal is © The Royal Society of Chemistry 2013

**4. Analysis of the AFM images of salt-etched Cu-MOFs surfaces (Fig. 2)**

The kinetics of salt etching process was probed by examining the effect of NaCl concentration on the Cu-MOF surface morphology using AFM. In this study, Cu-MOFs were treated by a series of salt solutions with concentrations of 0.57, 5.7, 57 and 570 mM respectively for 10 minutes prior to imaging.

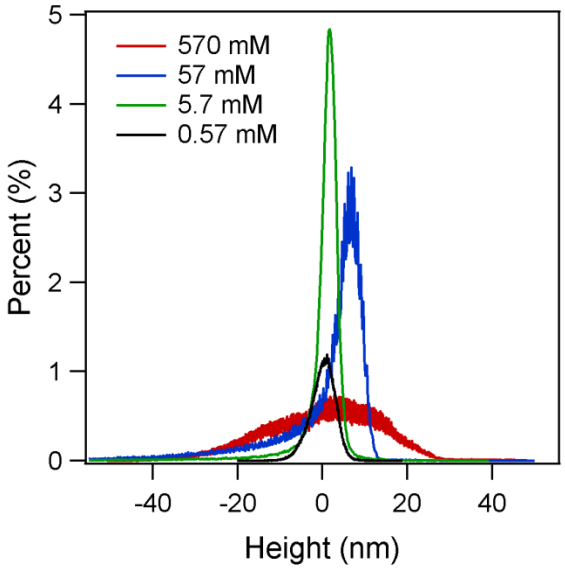


**Fig. S2** Height histogram of the AFM images (Fig. 2) of the Cu-MOFs treated by NaCl solutions with concentration of 0.57, 5.7, 57 and 570 mM. The plot is based on the depth analysis data obtained with the SPIP program.

**Table S2** Surface morphology evolution analysis based on Fig. 2 and S2. The peak to peak distance measures the distance between the minimum peak depth and depth at histogram maximum. All data are obtained with the SPIP program.

| Salt Concentration (mM) | Roughness ($R_q$, nm) | Peak to Peak Distance (nm) | Material Volume ($\mu m^3$) | Void Volume ($\mu m^3$) | Void Volume Fraction (%) |
|---|---|---|---|---|---|
| **0.57** | 3.02 | 39.07 | 0.081 | 0.076 | 48 |
| **5.7** | 6.92 | 115.86 | 0.307 | 0.158 | 34.0 |
| **57** | 12.9 | 137.59 | 0.351 | 0.201 | 36.4 |
| **570** | 13.4 | 100.44 | 0.204 | 0.199 | 49.4 |

**5. Gas sorption study of H-MOFs**

The $N_2$ sorption isotherms of H-MOFs were taken at both 77 K and 195 K (Fig. S3). Both isotherms show negative values indicating negligible gas sorption. The BET surface, 0.2528 $m^2/g$, calculated from $N_2$ sorption at 77 K, is indicative of negligible surface area or pores. Compared to the Cu-MOFs, in which the interpenetrated microporous structure exhibits certain $N_2$ sorption ability (Fig. S3A and S3B adapted from Ref. 1), the H-MOFs likely no longer have the interpenetrated networks but the broken ones.

The $CO_2$ sorption study of H-MOFs at 195 K shows selective $CO_2$ sorption over $N_2$ (Fig. S3D) and the value is about half of the one adsorbed by Cu-MOFs. Because the $CO_2$ sorption in these MOF structures is likely due to the chemical interaction between $CO_2$ and the available open metal sites, the reduced sorption also suggests the cleaving of original interpenetrated framework by salt etching.

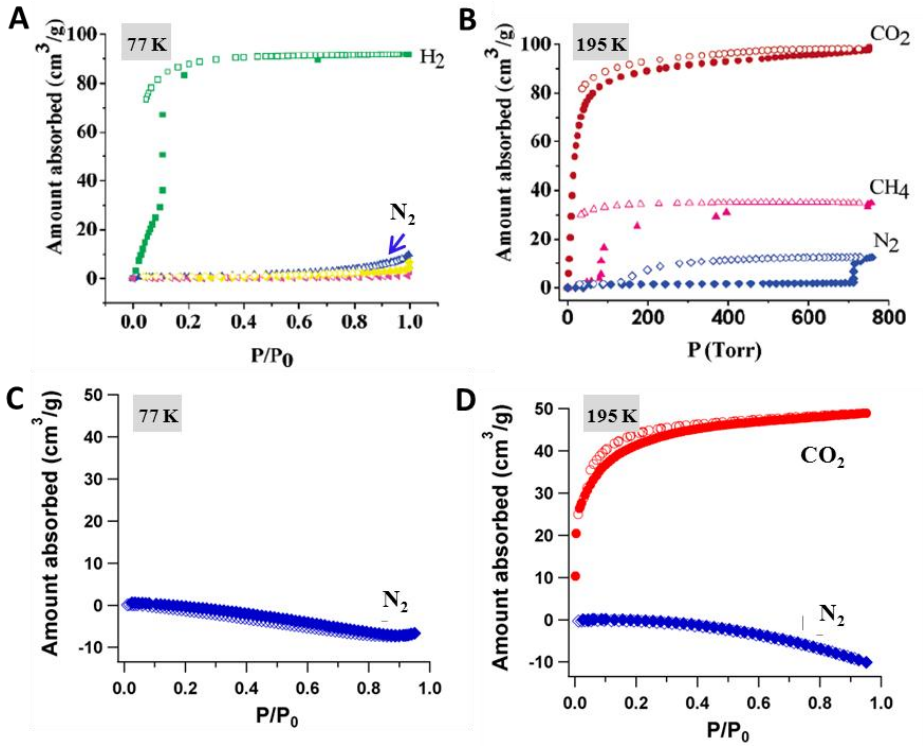


**Fig. S3** Gas sorption isotherms of Cu-MOFs and H-MOFs at 77 K and 195 K. (a) and (b) are gas sorption isotherms of Cu-MOFs adapted from Fig 2 in Ref. S1. In (a), the $H_2$, $N_2$, Ar, and CO isotherms are shown in green, blue, magenta, and yellow.

**6. Crystal structures of Cu-MOFs, H-MOFs, $CuCl_2$·(4,4'-Bpe) and CuFMA**

We carefully examined the powder XRD pattern of hairy MOFs (H-MOFs), which had no match in the existing crystal structure database. In order to find the chemical identity of H-MOFs, we synthesized a series of crystalline materials containing different combinations of Cu, fumarate ion ($FMA^{2-}$) and 4,4'-Bpe for matching purposes. After comparing their XRD patterns of these compounds (Fig. S3), we found the hairy MOFs held similar crystal structure with $CuCl_2$·(4,4'-Bpe) except for a few extra peaks, mainly at 16.5°, 19.4°, 20.3° and 25.7°.

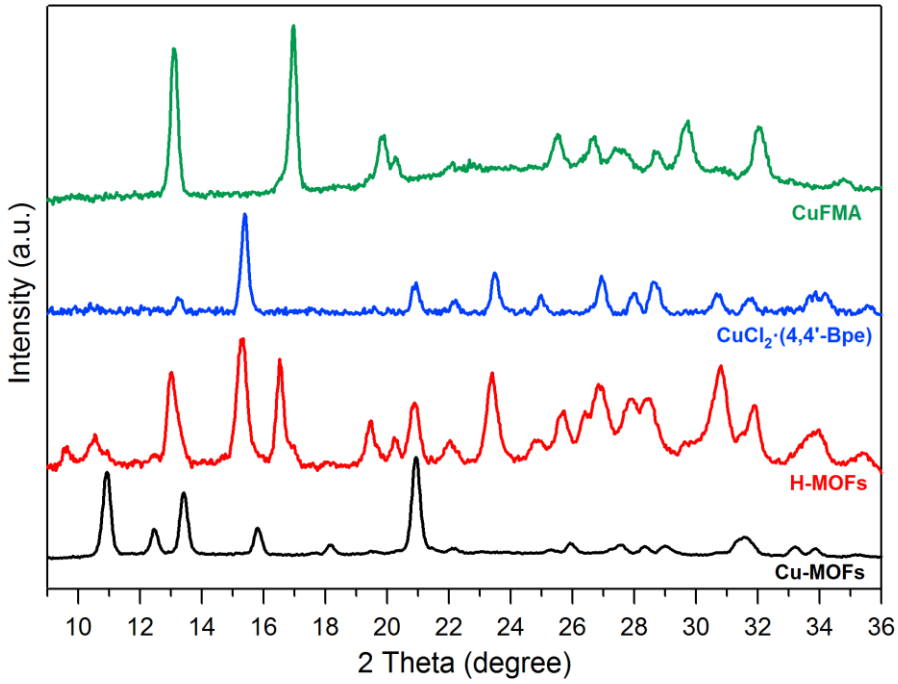


**Fig. S4** Powder XRD patterns of Cu-MOFs, H-MOFs, $CuCl_2$·(4,4'-Bpe) and CuFMA. H-MOFs show the characteristic diffraction peaks of both $CuCl_2$·(4,4'-Bpe) and CuFMA.

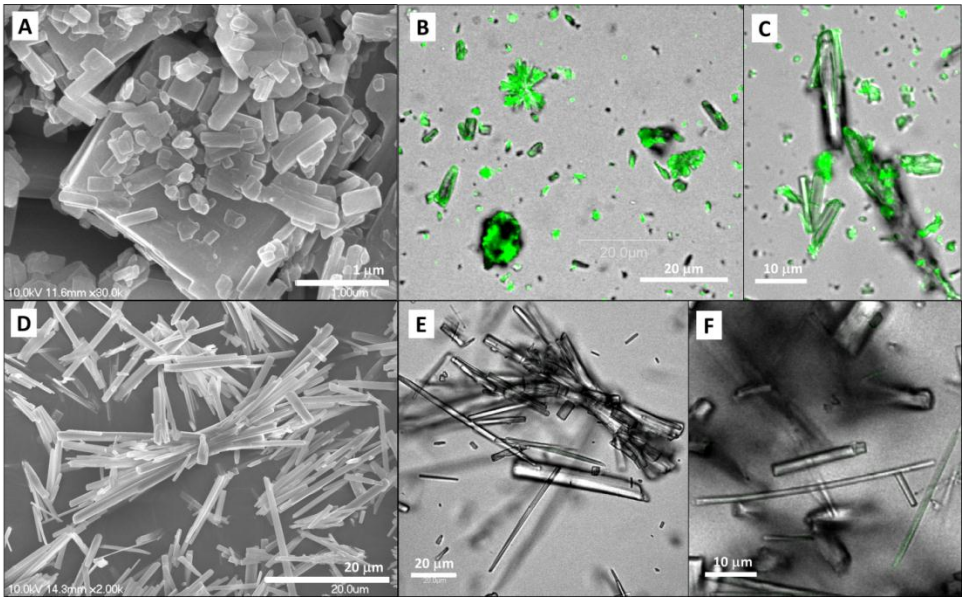


**Fig. S5** The morphologies of $CuCl_2$·(4,4'-Bpe) and CuFMA, and their interactions with GFP. (A) SEM image of $CuCl_2$·(4,4'-Bpe) showing rod-like structures coexisting with larger blocks; (B and C) Confocal fluorescent microscopic image of $CuCl_2$·(4,4'-Bpe) illustrating intense fluorescent response on the crystal surface, suggesting strong GFP adhesion; (D) SEM image of CuFMA showing uniform long rod-like morphology of the crystals and (E and F) Confocal fluorescent microscopic image of CuFMA with no detectable fluorescent signals, suggesting CuFMA is not active in binding GFP.

This journal is © The Royal Society of Chemistry 2013

**7. Behavior of Cu-MOFs and H-MOFs in biological media**

We compared the behaviors of Cu-MOF and hairy MOFs in Dulbecco's Modified Eagle Medium (DMEM) with added fetal bovine serum (FBS) and GFPs. Though DMEM, which contains monovalent and bivalent metal salts, can also drive the structure evolution of Cu-MOF similarly to NaCl solution, the Cu-MOF crystals in presence of FBS was found to retain most of their crystal structure integrity. This is likely due to the resistance of FBS which blocked the diffusion of salts into the solid frameworks.

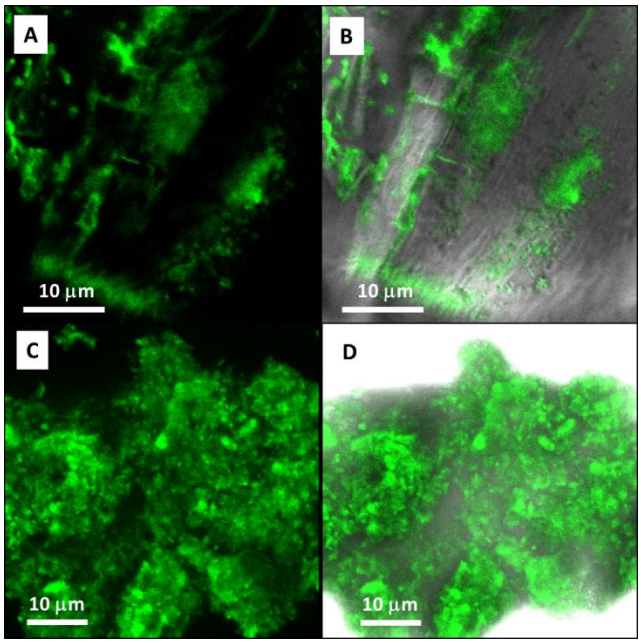


**Fig. S6** Confocal fluorescent microscopic images of Cu-MOFs and H-MOFs after soaking in FBS-containing DMEM and GFP for 1 week. (A and B) Fluorescent images of treated Cu-MOF unambiguously suggest the site-selective adhesion of GFPs on the defect sites of Cu-MOFs surface; (C and D) Fluorescent images of treated Cu-MOF-1 showing a uniform coverage of GFPs over the surface of H-MOFs, indicating the effectiveness of salt etching in enhancing bio-conjugation of Cu-MOF.

**References**

S1. B. L. Chen, S. Q. Ma, F. Zapata, F. R. Fronczek, E. B. Lobkovsky and H. C. Zhou, *Inorg. Chem.*, 2007, **46**, 1233-1236.
S2. M. E. Zaballa, L. A. Abriata, A. Donaire and A. J. Vila, *Proc. Natl. Acad. Sci. USA*, 2012, **109**, 9254-9259.